


Article

Genesis of the Dongpuzi Gold Deposit in the Liaodong Peninsula, NE China: Constraints from Geology, Fluid Inclusion, and C–H–O–S–Pb Isotopes

Cong Chen ^{1,2} , Taotao Wu ^{1,*}, Deming Sha ¹, Dongtao Li ¹, Zhongzhu Yang ^{1,2}, Jing Zhang ^{1,2} and Qingqing Shang ³

¹ Shenyang Center of Geological Survey, China Geological Survey, Shenyang 110034, China

² Key Laboratory of Deep Mineral Resources Exploration and Evaluation, Department of Natural Resource of Liaoning Province, Shenyang 110034, China

³ College of Earth Sciences, Jilin University, Changchun 130061, China

* Correspondence: wutaotao@mail.cgs.gov.cn

Abstract: The Dongpuzi deposit is an epithermal gold deposit located in the southern margin of the Shaozihe volcanic fault basin in the Liaodong Peninsula. On the basis of fluid inclusion and C–H–O–S–Pb isotope data, a metallogenic model is established for the Dongpuzi deposit. The mineralization at the Dongpuzi deposit has experienced quartz–pyrite (I), quartz–sulfide (II), and quartz–calcite (III) stages. The quartz from ore stage II has liquid-dominated aqueous inclusions, which have homogenization temperatures ranging from 113 to 162 °C and salinities varying from 3.2 to 9.6 wt% NaCl equiv. The quartz from the quartz–calcite stage has decreasing homogenization temperatures (106–143 °C) and salinities (2.7–6.9 wt% NaCl equiv.). The fluid inclusion data indicate that the gold ores were precipitated from low-temperature and low-salinity solutions, with an obvious decrease in temperature and salinity from ore stages II to III. The calculated $\delta^{18}\text{O}_{\text{water}}$ values for the quartz of ore stage II range from -14.71‰ to -13.31‰ , and the corresponding $\delta\text{D}_{\text{water}}$ values range from -103.3‰ to -96.1‰ , indicating that the ore-forming fluids could be of a meteoric origin. The calcite from ore stage III has $\delta^{13}\text{C}_{\text{V-PDB}}$ values of -4.5‰ to -4.2‰ and $\delta^{18}\text{O}_{\text{V-SMOW}}$ values of $+7.0\text{‰}$ to $+7.4\text{‰}$, indicating a mantle source for the carbon. The pyrite yielded $\delta^{34}\text{S}$ values of $+4.1\text{‰}$ to $+6.6\text{‰}$ and Pb isotopes consistent with those of the host trachyte porphyry and volcanic rocks of the Xiaoling Formation, which suggests that the S and Pb in gold ores were dominantly derived from the host trachyte porphyry and volcanic rocks of the Xiaoling Formation, with some combination of Paleoproterozoic metamorphic rocks of the Gaixian Formation. These results, together with the ore geology, indicate that the Dongpuzi deposit is a typical low-sulfidation epithermal gold deposit with important ore-forming materials input from the host trachyte porphyry, volcanic rocks of the Xiaoling Formation, and Paleoproterozoic metamorphic rocks of the Gaixian Formation. The Dongpuzi deposit was formed under an extensional setting related to the Early Cretaceous lithospheric extension and thinning of the eastern North China Craton.

Keywords: Dongpuzi gold deposit; C–H–O–S–Pb isotopes; fluid inclusions; low-sulfidation epithermal deposit; Liaodong Peninsula



Citation: Chen, C.; Wu, T.; Sha, D.; Li, D.; Yang, Z.; Zhang, J.; Shang, Q. Genesis of the Dongpuzi Gold Deposit in the Liaodong Peninsula, NE China: Constraints from Geology, Fluid Inclusion, and C–H–O–S–Pb Isotopes. *Minerals* **2022**, *12*, 1008. <https://doi.org/10.3390/min12081008>

Academic Editor: Léo Afraneo Hartmann

Received: 5 July 2022

Accepted: 9 August 2022

Published: 11 August 2022

Publisher's Note: MDPI stays neutral with regard to jurisdictional claims in published maps and institutional affiliations.



Copyright: © 2022 by the authors. Licensee MDPI, Basel, Switzerland. This article is an open access article distributed under the terms and conditions of the Creative Commons Attribution (CC BY) license (<https://creativecommons.org/licenses/by/4.0/>).

1. Introduction

The Liaodong Peninsula in the eastern North China Craton (NCC) is an important gold province in China that hosts numerous medium- and large-scale gold deposits, such as the Wulong, Baiyun, Sidaogou, Maoling, Wangjiaweizi, and Xiaotongjiapuzi deposits, contributing a total gold reserve of >220 t [1]. The gold deposits are mostly hosted within the Paleoproterozoic metamorphic rocks of the Liaohe Group, structurally controlled by fault zones and associated with Mesozoic granitic intrusions [2–4]. The gold deposits have been broadly classified into the quartz vein type, represented by the large-scale Wulong

deposit, and the fracture-controlled disseminated type, represented by the large-scale Sidaogou deposit [2]. However, except for the Mesozoic intrusive magmatic-hydrothermal gold deposits, the volcanic-hosted epithermal gold ore system is poorly mentioned in the Liaodong Peninsula.

The Dongpuzi gold deposit is a gold vein deposit occurring within the Shaozi River volcanic fault basin in the Xiuyan area, the northern part of the Liaodong Peninsula. Chen [5] first described the geology and ore-forming conditions of this deposit and proposed that it belongs to an epithermal gold deposit related to the host trachyte porphyry. Zhang et al. [6] recognized the mineralizing fluids with low temperatures (90~240 °C) and low salinities (0.35~6.17 wt% NaCl equiv.) and proposed a mixed magmatic and meteoric origin based on the limited fluid inclusion studies and H–O–S isotope data. Jiang [7] proposed that the basement rocks of the Liaohe Group may provide some ore-forming components for the Dongpuzi gold mineralization. However, the previous research lacked detailed investigations on petrography, mineralogy, and paragenesis, and the conclusions were based on limited microthermometric and isotopic data. Thus, the characteristics and origins of ore-forming fluids, sources of ore-forming materials, and genetic relationships between the Dongpuzi gold mineralization and Early Cretaceous volcanic rocks remain poorly known.

Based on field observation and ore geology, this paper carries out systematic fluid inclusion studies and presents new C–H–O–S–Pb isotopes for the Dongpuzi gold deposit. These new data provide further constraints on the characteristics and sources of the ore-forming fluids and materials, which allows a better understanding of the ore genesis of the Dongpuzi gold deposit. Finally, a tectonic–metallogenic model is established for the Dongpuzi gold mineralization.

2. Geological Background

2.1. Regional Geology

The Huanghuadianzi–Dayingzi–Shaozi River region is located in the eastern part of the NCC, on the western margin of the Paleo-Pacific Plate (Figure 1a). The rocks exposed in the area mainly comprise Paleoproterozoic metamorphic rocks of the Liaohe Group and granitic and mafic intrusions, and a series of Mesozoic intrusive and volcanic rocks, as well as minor Late Triassic epimetamorphic rocks of the Cuocaogou Formation (Figure 1b). The Paleoproterozoic Liaohe Group includes the Lieryu, Gaojiayu, Dashiqiao, and Gaixian formations in the area, which have been metamorphosed to the greenschist to lower amphibolite facies and locally to the granulite facies [8]. The Lieryu and Gaojiayu formations are composed dominantly of fine-grained felsic gneiss, amphibolite, and mica–quartz schist. The Dashiqiao Formation consists of dolomitic marble intercalated with minor carbonaceous slate and mica schist [9]. The uppermost Gaixian Formation mainly comprises andalusite–cordierite–mica schist, phyllite, sillimanite–mica schist, and staurolite–mica schist, with minor marble and quartzite. The Paleoproterozoic Liaoji granitoids are widely developed in the area and mainly include deformed monzogranitic gneiss, undeformed porphyritic monzogranite, granite, and alkaline syenite [10].

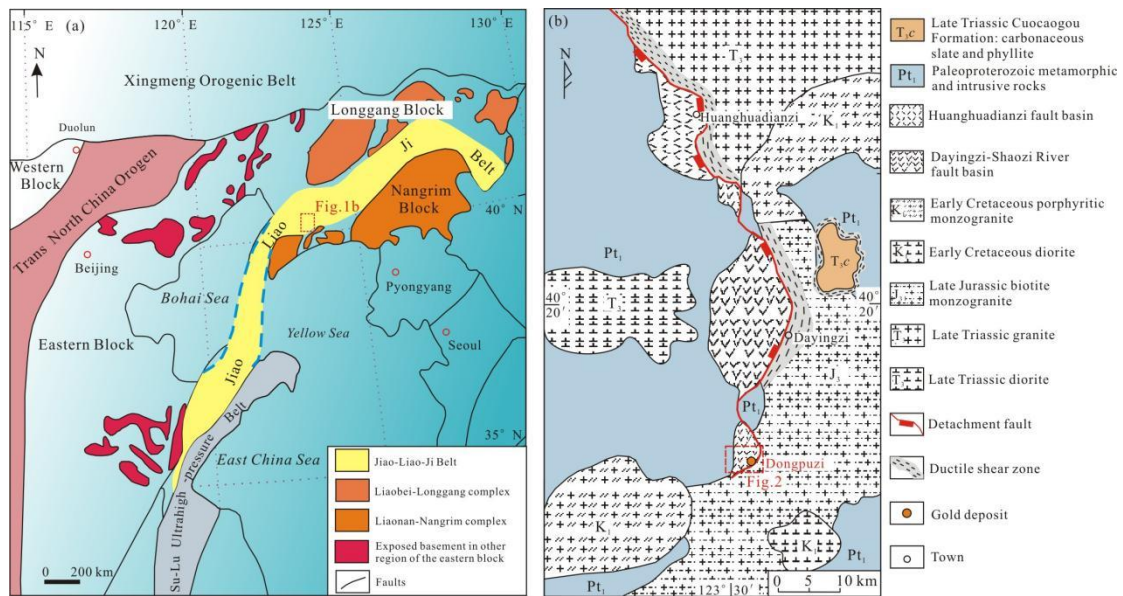


Figure 1. Geological and tectonic map of the eastern NCC (a), modified from [8]. A sketch map of the Huanghuadianzi–Dayingzi–Shaozi River area, Liaodong Peninsula (b), modified from [11]. The location of Figure 2 has been marked by a red rectangle.

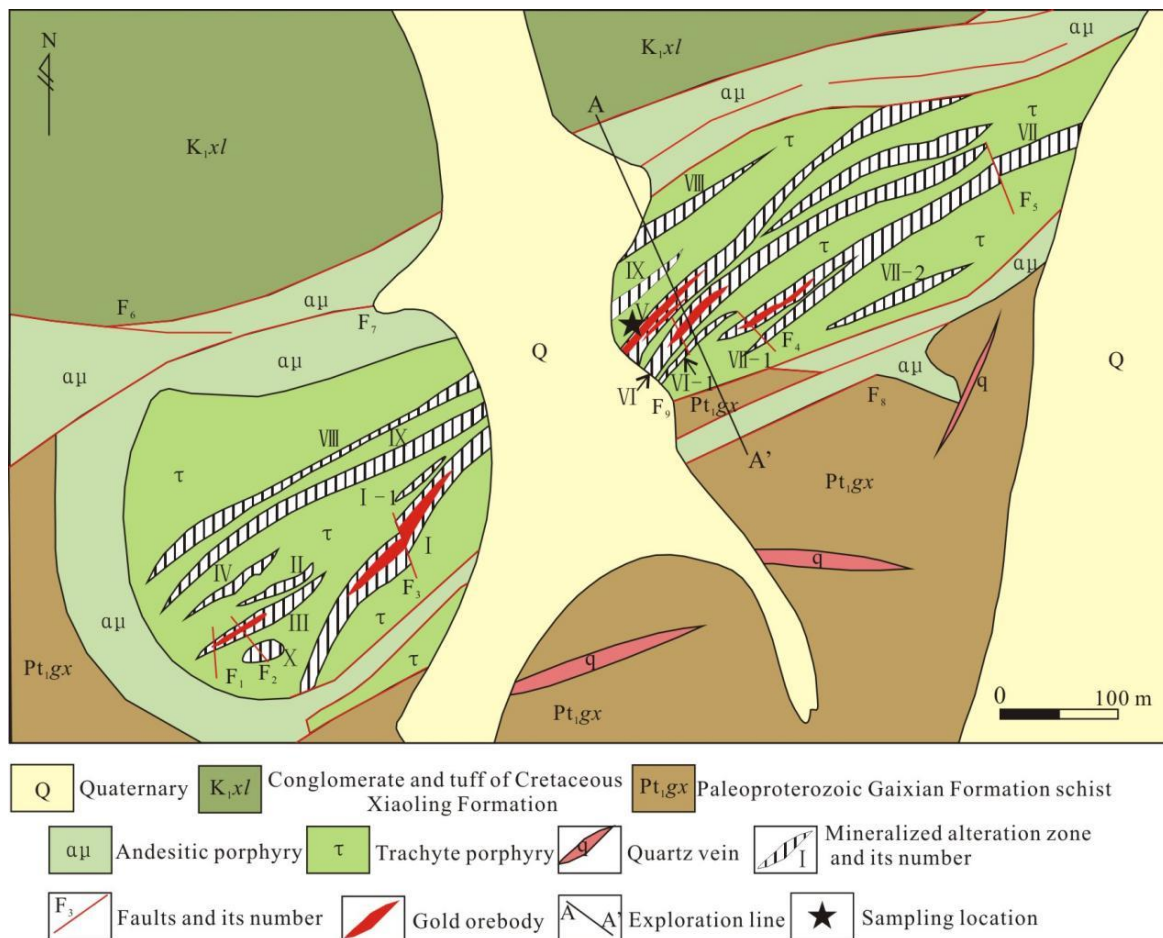


Figure 2. Geological map of the Dongpuzi gold deposit (modified from [5]).

Since the Late Triassic period, the area has experienced intensive tectonic and magmatic activities as an important part of the Circum-Pacific tectono-magmatic zone [12]. The Late Triassic Cuocaogou Formation occurs as erosion residue overlying the Paleoproterozoic metamorphosed sedimentary and volcanic successions of the Liaohe Group and includes carbonaceous slate and phyllite. Intrusive rocks in the area are dominantly Late Triassic diorite and monzogranite, Late Jurassic biotite monzogranite, and Early Cretaceous porphyritic monzogranite and diorite [11,12] (Figure 1b). The tectonic structure in the area is mainly dominated by the Huanghuadianzi–Dayingzi–Shaozi River extensional structure, which is composed of three major units: the extensional fault basins (Huanghuadianzi, Dayingzi, and Shaozi Rivers) in the hanging wall, detachment fault, and Early Cretaceous granitic plutons in the lower plate [9,13]. The extensional fault basins are mainly filled with the volcanic sedimentary rocks of the Early Cretaceous Xiaoling Formation, which include basalt, andesitic basalt, andesite, rhyolite, conglomerate, tuffaceous sandstone, and tuff.

The detachment fault extends from the Huanghuadianzi in the north, through the Dayingzi, to Shaozi River in the south, with a length of about 70 km. The fault always dips SW at 24° and develops a series of brittle high-angle normal faults and ductile shear zones in the Mesozoic granitic plutons [11,13] (Figure 1b).

2.2. Geology of the Dongpuzi Orefield

The Dongpuzi gold deposit is located in the southernmost part of the Huanghuadianzi–Dayingzi–Shaozi River extensional structure, in the south margin of the Shaozi River volcanic fault basin (Figure 1b). Strata in the Dongpuzi gold field consist mostly of the Gaixian Formation of the Paleoproterozoic Liaohe Group and Early Cretaceous Xiaoling Formation (Figure 2). The Gaixian Formation is mainly composed of biotite schist, two-mica schist, and sillimanite biotite schist [5]. The Xiaoling Formation comprises limestone, coarse sandstone, and tuff. The Cenozoic stratigraphy is dominated by alluvial deposits.

The tectonic structures of the Dongpuzi orefield include a series of NE–SW- to NNE–SSW-trending faults and minor NW–SE- to NNW–SSE-trending faults (Figure 2). The NE–SW- to NNE–SSW-trending faults always dip NW at 50–70° and are characterized by multi-periodic activities. The faults control the emplacement of ore-hosting trachyte porphyry and post-ore andesitic porphyry and lead to the formation of several joints and fractures. The joints and fractures are marked by intensive mineralization and alteration and control the formation of the Dongpuzi gold-bearing quartz veins. The NW–SE- to NNW–SSE-trending faults cut the mineralized alteration zones and gold orebodies.

The intrusive rocks are mainly Early Cretaceous trachyte porphyry and andesitic porphyry, which are distributed in the middle part of the Dongpuzi orefield. The trachyte porphyry was emplaced along the NE–SW- to NNE–SSW-trending faults and hosted the mineralized alteration zones and gold orebodies. The andesitic porphyry intruded into the Gaixian Formation and trachyte porphyry, as well as the gold orebodies (Figures 2 and 3).

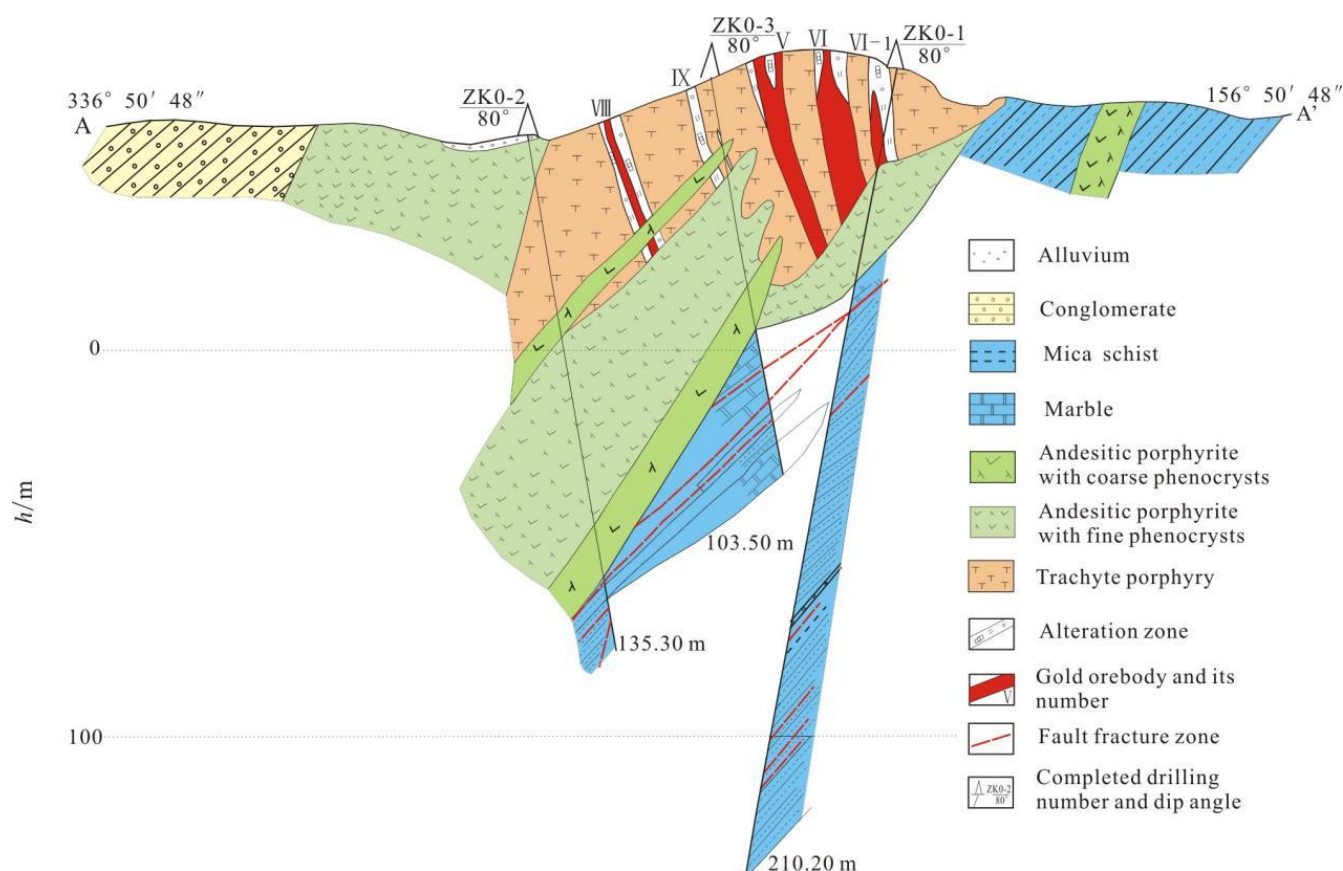


Figure 3. Geological cross section of the No.0 exploration line in the Dongpuzi gold deposit (modified after [14]; the location of the No.0 exploration line is referred as A-A' in Figure 2).

3. Ore Deposit Geology

The Dongpuzi gold deposit consists of 13 mineralized alteration zones (No. I, I-1, II, III, V, V-1, VI, VI-1, VIII, IX, X, etc.; Figure 2), which contain 30 gold orebodies, with an average grade of 5 gt^{-1} [14]. The gold orebodies are hosted within the Early Cretaceous trachyte porphyry (Figures 2 and 3) and structurally controlled by NE–SW- to NNE–SSW-trending faults and fracture zones. Gold mineralization occurs mainly as pyrite–sericite–quartz-altered rocks and auriferous quartz–pyrite veins and veinlets. The major orebodies are No. V and No. VI, which account for more than 77% of the total metal reserves of the Dongpuzi deposit (Figure 3) [14].

The ore mineral assemblage is mainly pyrite, with minor chalcopyrite, sphalerite, tetrahedrite, native gold, and electrum (Figure 4). The nonmetallic minerals observed in the ores include quartz, sericite, calcite, kaolin, and chlorite (Figure 4). Native gold and electrum generally occur as grains in inclusions or along fractures within pyrite and quartz grains (Figure 4i). The ore minerals are characterized by subhedral to anhedral granular (Figure 4d,e), metasomatic (Figure 4e,f), poikilitic, and cataclastic textures. They occur either in veins (Figure 4a), veinlets, or stockworks (Figure 4b) or have veinlet-disseminated, disseminated, or miarolitic structures (Figure 4b).

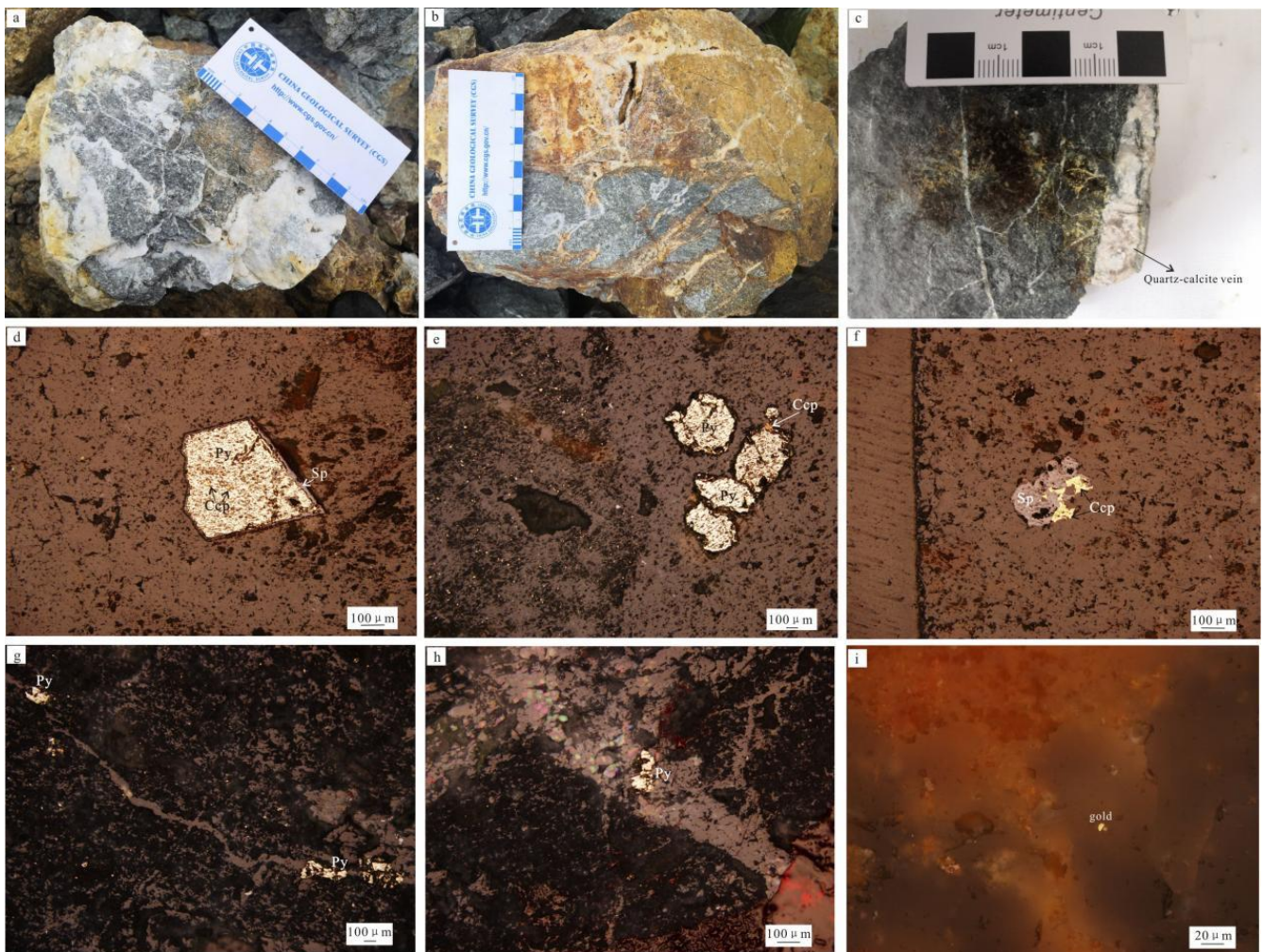


Figure 4. Photographs and microphotographs of the Dongpuzi gold ores. (a): The quartz–pyrite-vein-type ore. (b): The gold ores characterized by a miarolitic structure. (c): The quartz–calcite vein cut through the altered trachyte porphyry. (d,e): The subhedral pyrite was metasomatized by later chalcopyrite and sphalerite. (f): The sphalerite was metasomatized by later chalcopyrite. (g,h): The anhedra pyrite within the quartz veinlet. (i): The gold mineral within the quartz veins. Abbreviations: Ccp = chalcopyrite, Py = pyrite, Qz = quartz, and Sp = sphalerite.

The wall-rocks record various types of alterations, which include sericitization, silicification, carbonatization, kaolinization, and chloritization. Silicification usually manifests as quartz veins, veinlets, or stockwork. Carbonatization mainly occurs as quartz–calcite veins and locally cut the early-stage gold-bearing quartz veins. In addition, the wall-rock alteration displays clear spatial zonation, which can be classified into three zones from the gold orebody to wall-rocks: an inner silicification–pyritization–sericitization zone, a middle silicification–sericitization–kaolinization zone, and an external silicification–chloritization zone [15].

On the basis of the paragenetic assemblages and crosscutting relationships, gold mineralization in the Dongpuzi deposit can be divided into three hydrothermal stages: the quartz–pyrite stage (I), the quartz–sulfide stage (II), and the quartz–calcite stage (III). The quartz–pyrite stage forms large amounts of quartz and sericite and minor subhedral pyrite, with little or no gold (Figure 4a). The quartz–sulfide stage represents the main metallogenic stage of gold, which is characterized by quartz, pyrite, chalcopyrite, sphalerite, and minor native gold and electrum (Figure 4b,d–f,i). The quartz is always smoky gray and occurs as quartz veins, veinlets, or stockworks within the trachyte porphyry (Figure 4b,g,h). The

euhedral–subhedral pyrite grains are locally metasomatized by later chalcopyrite and sphalerite (Figure 4d,e). The quartz–calcite stage is characterized by quartz and calcite occurring as veins that crosscut the earlier quartz–sulfide veins (Figure 4c).

4. Sampling and Analytical Methods

The samples analyzed for fluid inclusion studies and C–H–O–S–Pb isotopes herein were collected from the No.V gold orebody derived from the underground mine. The fresh trachyte porphyry samples were collected in the mine dump for analysis of the Pb isotope. Descriptions of the samples are presented in Table 1.

Table 1. Sample characteristics of the Dongpuzi gold deposit.

Sample Number	Mineral/Sample	Mineralization Stage	Sample Location and Characteristics	Analysis
21dpl-1	Quartz	Quartz–sulfide	Quartz from intensely silicified trachyte porphyry	Fluid inclusion
21dpl-2	Quartz	Quartz–sulfide	Quartz veins within the trachyte porphyry, where sericitization and silicification occur	
21dpl-3	Quartz	Quartz–sulfide	Quartz–calcite veins cutting the trachyte porphyry, where sericitization and silicification occur	
21dpl-5	Quartz	Quartz–calcite	Quartz–calcite veins cutting the trachyte porphyry, where sericitization and silicification occur	
21DP-1	Quartz	Quartz–calcite	Quartz–calcite vein cutting the trachyte porphyry, where sericitization and silicification occur	H–O isotopes
21DP-2	Quartz	Quartz–sulfide	Quartz from intensely silicified trachyte porphyry	
21DP-3	Quartz	Quartz–sulfide	Quartz veins within the trachyte porphyry, where sericitization and silicification occur	
21DP-4	Quartz	Quartz–sulfide	Quartz veins within the trachyte porphyry, where sericitization and silicification occur	
21DP-5	Quartz	Quartz–sulfide	Quartz veins within the trachyte porphyry, where sericitization and silicification occur	
21DP-6	Calcite	Quartz–calcite	Quartz–calcite vein cutting the trachyte porphyry, where sericitization and silicification occur	C–O isotopes
21DP-7	Calcite	Quartz–calcite		
21DP-8	Calcite	Quartz–calcite		
DP-2	Pyrite	Quartz–sulfide	Pyrite within intensely silicified trachyte porphyry	S–Pb isotopes
DP-3	Pyrite	Quartz–sulfide		
DP-4	Pyrite	Quartz–sulfide		
21DP-9	Pyrite	Quartz–sulfide		
21DP-10	Pyrite	Quartz–sulfide		
DPX-1	Trachyte porphyry	-	Trachyte porphyry with little or no alteration and mineralization	Pb isotope
DPX-2	Trachyte porphyry	-		
DPX-3	Trachyte porphyry	-		
DPX-4	Trachyte porphyry	-		
DPX-5	Trachyte porphyry	-		

Note: “-” in the list of “Mineralization stage” refers to no correspondence between the trachyte porphyry and the mineralization stage.

4.1. Fluid Inclusion Petrography and Microthermometry

Quartz from intensely silicified trachyte porphyry (21dpl-1), quartz veins (21dpl-2, 3) in the gold ores from the main metallogenic stage (II), and quartz from quartz–calcite veins (21dpl-5) from the late ore stage (III) were chosen for fluid inclusion studies to determine the characteristics of the ore-forming fluids of ore stages II and III.

The petrographic observation and microthermometry of fluid inclusions were performed at the Analytical Laboratory of the Beijing Research Institute of Uranium Geology, Beijing, China. Microthermometric measurements were conducted on a LINKAM THMS-600 type heating–freezing stage, which has a temperature measurement range of -196 °C to $+600$ °C. During the heating and freezing process, the temperature control rate was less than

5 °C/min, and the rate decreased to less than 1 °C/min when the phase transformation was about to occur.

4.2. Isotope Analysis

Quartz grains from quartz veins (21DP-1; ore stage II), silicified trachyte porphyry (21DP-2; ore stage II), and quartz–calcite veins (21DP-3, -4, -5; ore stage III) were analyzed for H–O isotopes; and calcite grains from quartz–calcite veins (21DP-6, -7, -8; ore stage III) were analyzed for C–O isotopes to determine the source of the ore-forming fluids. Pyrite grains from intensely silicified trachyte porphyry (DP-2, -3, -4) and quartz veins (21DP-9, -10) of ore stage II were analyzed for S and Pb isotopes to constrain the source of ore-forming materials. The trachyte porphyry samples with little or no alterations that host the No.V gold orebody were analyzed for the Pb isotope to reveal the relationship between the gold ores and host rocks.

C, H, O, S, and Pb isotopes were analyzed at the Analytical Laboratory of the Beijing Research Institute of Uranium Geology, Beijing, China. The quartz, calcite, and pyrite mineral grains from ore stages II and III with a purity of >98% were ground to 40~60 mesh for analyses of C, H, and O isotopes. Furthermore, the fresh trachyte porphyry samples were crushed to 200 mesh for analysis of the Pb isotope.

H and O isotopic compositions of fluid inclusions within the quartz crystals and C and O isotopic compositions of those in calcite crystals were measured using a MAT-253 mass spectrometer. The isotopic results were standardized by Vienna-Standard Mean Ocean Water (V-SMOW) for H and O isotopes and the Vienna-Peedee Belemnite (V-PDB) standard for the C isotope. The analytical precisions were better than $\pm 1\%$ for δD , $\pm 0.2\%$ for $\delta^{18}O$, and $\pm 0.2\%$ for $\delta^{13}C$.

S isotopic compositions of five pyrite samples were determined using a Delta V Plus mass spectrometer. The S isotopic results were standardized by Vienna-Canyon Diablo Troilite (V-CDT), and analytical precision was estimated to be $\pm 0.2\%$.

Pb isotope analyses of five pyrite and five trachyte porphyry samples were conducted using an ISOPROBE-T thermal ionization mass spectrometer. The Pb isotopic ratios were corrected using NBS SRM 981 [16], and the Pb isotope uncertainties were reported as $\pm 2\sigma$. The measurement accuracy was <0.05% for $^{204}Pb/^{206}Pb$ and <0.005% for $^{208}Pb/^{206}Pb$ with 1 μg of lead. The specific procedures for C, H, O, S, and Pb isotopic analyses are described by Guo et al. [17].

5. Results

5.1. Fluid Inclusions

Fluid inclusions within the quartz crystals in gold ores formed during ore stages II and III were analyzed. Petrographic observations indicate that fluid inclusions are common in quartz crystals at room temperature and mainly include three types: (1) liquid-only aqueous inclusions (L-only), (2) vapor-only aqueous inclusions (V-only), and (3) bi-phase (liquid and vapor) aqueous inclusions dominated by liquid (L-dominated) and finally homogenized to liquid (Figure 5). The three types of fluid inclusions occur in both ore stages II and III.

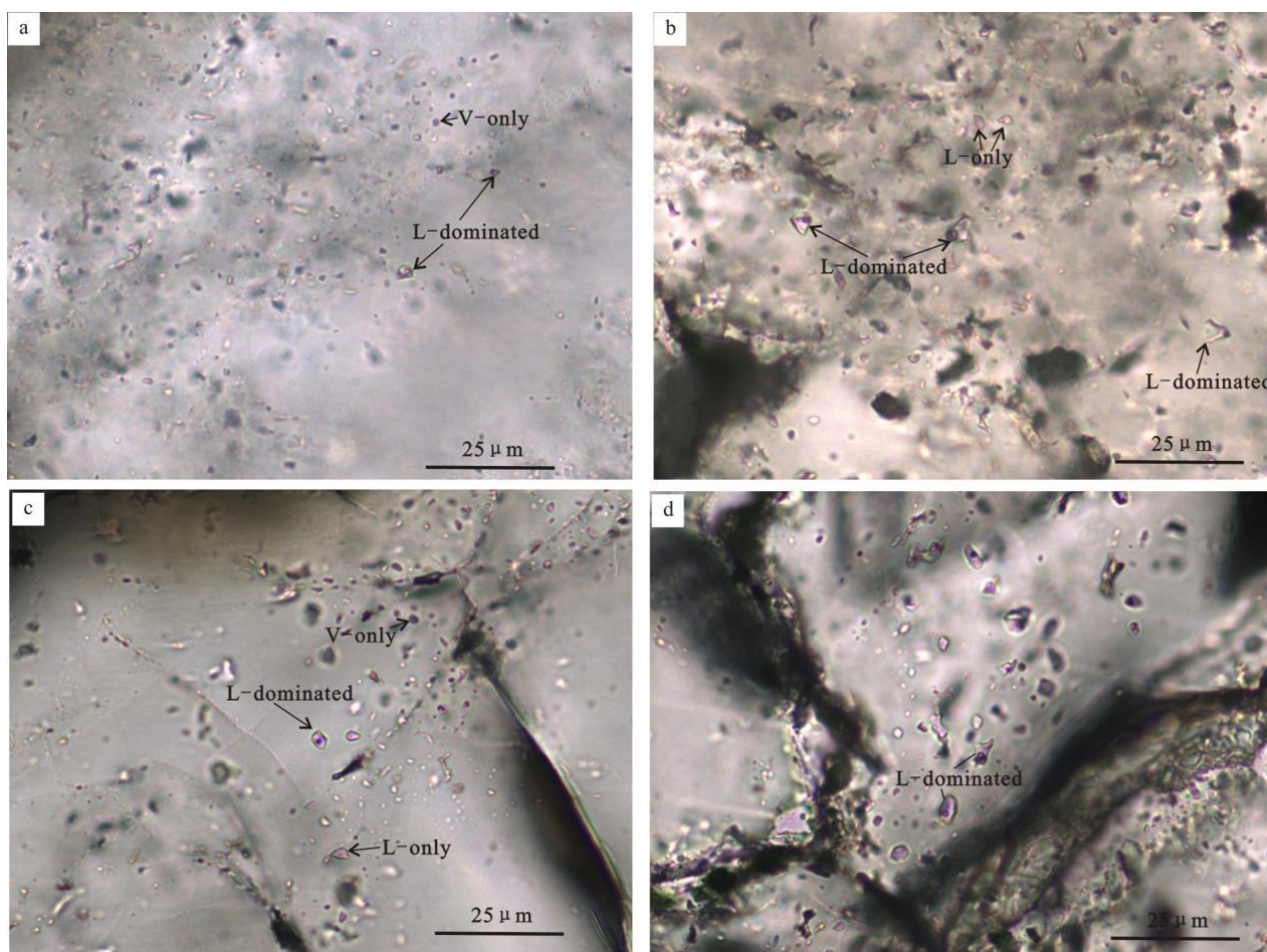


Figure 5. Photomicrographs of the fluid inclusions for the Dongpuzi gold deposit. (a,b): V-only, L-only, and L-dominated fluid inclusions within the quartz crystal from ore stage II; (c,d): V-only, L-only, and L-dominated fluid inclusions within the quartz crystal from ore stage III).

Ore stage II: L-dominated fluid inclusions are distributed in groups or scattered, and they are subrounded or irregularly polygonal in shape, with sizes of 2~7 μm (Figure 5a,b). They mostly contain a vapor phase that occupies 5~10 vol%. L-only fluid inclusions are elliptical and irregular in shape, with sizes of 2~5 μm (Figure 5b). V-only fluid inclusions generally exhibit obvious dark halos under the microscope and are dispersively distributed. They are mostly round or elliptical in shape, with sizes of 3~5 μm (Figure 5a).

Ore stage III: L-dominated fluid inclusions are mostly rounded and subrounded in shape, and their sizes range from 1 to 13 μm , most of which are 3~8 μm (Figure 5c,d). The volume of vapor in the L-dominated fluid inclusions of ore stage III is 5~10%. L-only and V-only fluid inclusions often coexist with the L-dominated fluid inclusions in the same quartz crystal. L-only fluid inclusions are generally scattered in the quartz crystal and are subrounded or irregular polygonal in shape, with sizes of 2~8 μm (Figure 5c). V-only fluid inclusions are distributed in groups or scattered, and most of them are elliptical in shape. Their sizes usually vary from 1 to 6 μm (Figure 5c).

The primary L-dominated fluid inclusions occurring in ores of stages II and III were chosen for microthermometry analysis. Due to their poor visibility or small sizes, few ice-melting temperatures of L-dominated fluid inclusions have been measured in this study. The homogenization and ice-melting temperatures of fluid inclusions and related calculation equations are summarized in Table 2.

Table 2. Microthermometric data of the L-dominated fluid inclusions for the Dongpuzi gold deposit.

Sample Number	Host Mineral	Fluid Inclusion Types	Homogeneous Temperatures ($T_H/^\circ\text{C}$)	Ice-Melting Temperatures ($T_{ice}/^\circ\text{C}$)	Salinity (wt% NaCl)
21dpl-1	Quartz	L-dominated	113~151 (17)	6.3~4 (8)	6.4~9.6 (8)
21dpl-2	Quartz	L-dominated	109~162 (27)	5.3~1.9 (13)	3.2~8.3 (13)
21dpl-3	Quartz	L-dominated	110~161 (24)	6~5.9 (5)	9~9.2 (5)
21dpl-5	Quartz	L-dominated	106~143 (25)	4.3~1.6 (6)	2.7~6.9 (6)

Note: The number in the parentheses means the number of measurements; the equation for salinity calculations: $S = 0 + 1.76985 \times T_{ice} - 0.042384 \times T_{ice}^2 + 0.00052778 \times T_{ice}^3$ ([18]).

L-dominated fluid inclusions within quartz crystals of ore stage II have homogenization temperatures ranging from 113 to 162 °C, with an average of 134 °C (Figure 6a). The salinities of these inclusions vary from 3.2 to 9.6 wt% NaCl equiv. based on the final ice-melting temperatures of −6.3 to −1.9 °C.

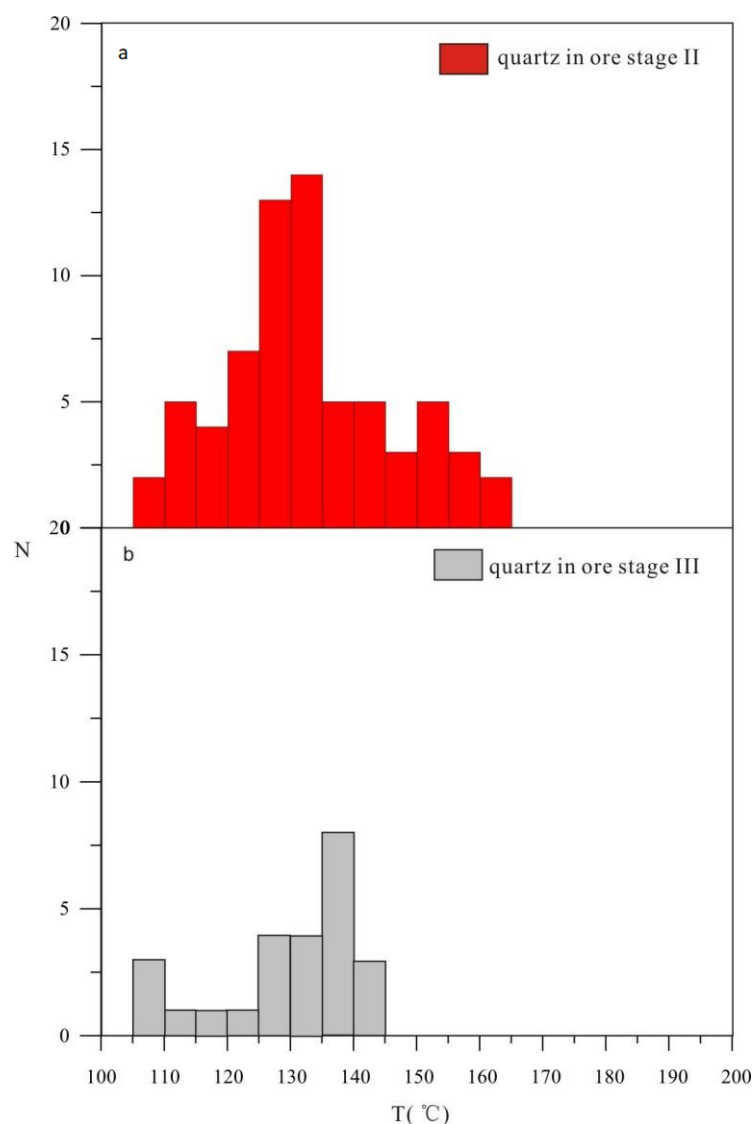


Figure 6. Histograms of homogenization temperatures of fluid inclusions of the Dongpuzi gold deposit. ((a): homogenization temperatures of fluid inclusions from the ore stage II; (b): homogenization temperatures of fluid inclusions from the ore stage III).

The homogenization temperatures of L-dominated fluid inclusions within quartz crystals of ore stage III vary from 106 to 143 °C, with an average of 129 °C (Figure 6b). The

salinities of these fluid inclusions vary from 2.7 to 6.9 wt% NaCl equiv. based on the final ice-melting temperatures of -4.3 to -1.6 °C.

5.2. C–H–O Isotopic Compositions

The C–H–O isotopic data and relative fractionation equations of the Dongpuzi gold deposit are presented in Table 3 and plotted in Figure 7. Four quartz samples of ore stage II have $\delta^{18}O_{V-SMOW}$ and δD_{water} values of $+2.9\text{‰}$ to $+4.3\text{‰}$ and -103.3‰ to -96.1‰ , respectively, with corresponding $\delta^{18}O_{water}$ values of -14.71‰ to -13.31‰ . One quartz sample of ore stage III has $\delta^{18}O_{V-SMOW}$ and δD_{water} values of $+4.4\text{‰}$, and -103.9‰ , respectively, with corresponding $\delta^{18}O_{water}$ values of -13.62‰ . Three calcite samples from ore stage III have $\delta^{13}C_{V-PDB}$ values of -4.5‰ to -4.2‰ and $\delta^{18}O_{V-SMOW}$ values of $+7.0\text{‰}$ to $+7.4\text{‰}$.

Table 3. C–H–O isotope data of the Dongpuzi gold deposit.

Sample Number	Mineral	T (°C)	δD_{V-SMOW} (‰)	$\delta^{13}C_{V-PDB}$ (‰)	$\delta^{18}O_{V-SMOW}$ (‰)	$\delta^{18}O_{H_2O-SMOW}$ (‰)
21DP-1	Quartz	129	-103.9	-	4.4	-13.62
21DP-2		-	-94.2	-	4.3	-13.31
21DP-3		133	-94.9	-	4.2	-13.41
21DP-4		-	-103.3	-	3.7	-13.91
21DP-5		-	-96.1	-	2.9	-14.71
21DP-6	Calcite	-	-	-4.2	7.4	-
21DP-7		129	-	-4.5	7.2	-
21DP-8		-	-	-4.3	7	-

Note: The equilibrium temperatures for each stage are based on the fluid inclusion studies in this paper. The fractionation equation for $\delta^{18}O_{water}$ calculation: $1000\ln\alpha_{quartz-water} = 3.38 \times 10^6/T^2 - 2.9$ ([19]). The “-” in the table means no analytical results.

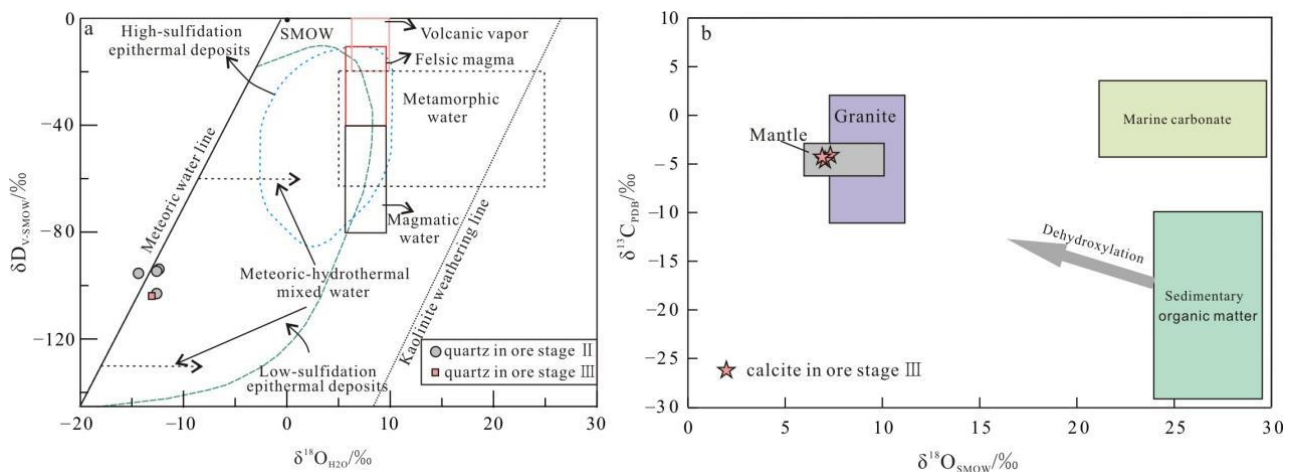


Figure 7. Diagrams of $\delta D-\delta^{18}O$ (a) and $\delta C-\delta^{18}O$ (b) ((a) is modified from [20,21]; the fields for the epithermal deposits and meteoric-hydrothermal mixed water are from [22] and [23], respectively; (b): the carbonate fields of marine carbonate, sedimentary organic carbon, and magma-mantle carbonate are from [24] and [25], respectively).

5.3. S Isotopic Compositions

The S isotopic data of the Dongpuzi gold deposit are presented in Table 4 and plotted in Figure 8a,b. Five pyrite samples yield relatively homogeneous S isotopic compositions with $\delta^{34}S_{V-CDT}$ values ranging from $+4.1\text{‰}$ to $+6.6\text{‰}$.

Table 4. Pyrite S–Pb isotopic data of the Dongpuzi gold deposit.

Sample Number	$\delta^{34}\text{S}_{\text{V-CDT}}/\text{‰}$	$^{208}\text{Pb}/^{204}\text{Pb}$	Std Err	$^{207}\text{Pb}/^{204}\text{Pb}$	Std Err	$^{206}\text{Pb}/^{204}\text{Pb}$	Std Err
DP-2	6.5	38.798	0.003	15.636	0.001	18.069	0.001
DP-3	5.5	38.827	0.004	15.638	0.002	18.039	0.002
DP-4	6.6	38.798	0.006	15.641	0.001	18.07	0.001
21DP-9	6	38.557	0.007	15.595	0.002	17.918	0.002
21DP-10	4.1	38.819	0.007	15.64	0.003	18.046	0.003

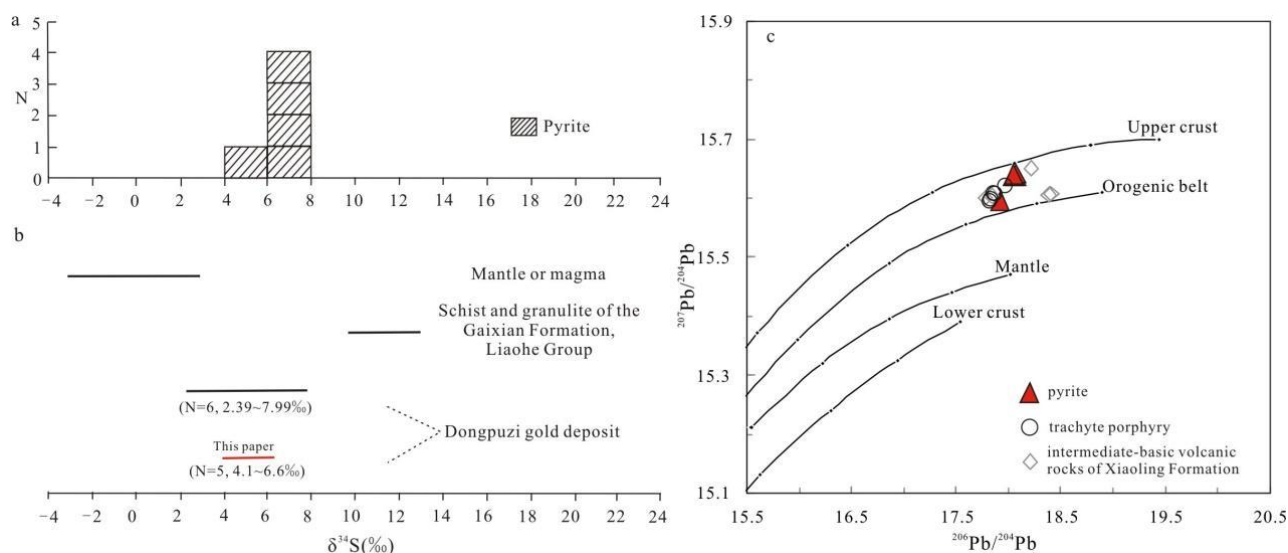


Figure 8. Histogram of the S isotope in the Dongpuzi gold deposit (a) and comparison of $\delta^{34}\text{S}$ values between the Dongpuzi deposit and associated geological bodies (b). The S isotopic data of Dongpuzi gold deposit are from this paper and [15]; data of the metamorphic rocks of the Gaixian Formation and mantle or deep magma are from [26,27], respectively. The Pb evolution curves for Dongpuzi gold ores (c). The data of intermediate-basic rocks of the Xiaoling Formation are from [28].

5.4. Pb Isotopic Compositions

The Pb isotopic compositions of pyrite and trachyte porphyry samples are given in Tables 4 and 5 and plotted in Figure 8c. Five pyrite samples have $^{206}\text{Pb}/^{204}\text{Pb}$ ratios of 17.918–18.07, $^{207}\text{Pb}/^{204}\text{Pb}$ ratios of 15.595–15.641, and $^{208}\text{Pb}/^{204}\text{Pb}$ ratios of 38.557–38.827 (Table 4). Five trachyte porphyry samples have $^{206}\text{Pb}/^{204}\text{Pb}$ ratios of 17.955–17.848, $^{207}\text{Pb}/^{204}\text{Pb}$ ratios of 15.595–15.621, and $^{208}\text{Pb}/^{204}\text{Pb}$ ratios of 38.963–39.116 (Table 5).

Table 5. Pb isotopic data of trachyte porphyry in the Dongpuzi gold deposit.

Sample Number	Sample	Age/Ma	$^{208}\text{Pb}/^{204}\text{Pb}$	Std Err	$^{207}\text{Pb}/^{204}\text{Pb}$	Std Err	$^{206}\text{Pb}/^{204}\text{Pb}$	Std Err	$(^{208}\text{Pb}/^{204}\text{Pb})_i$	$(^{207}\text{Pb}/^{204}\text{Pb})_i$	$(^{206}\text{Pb}/^{204}\text{Pb})_i$
DPX-1	Trachyte porphyry	130	39.375	0.004	15.625	0.002	18.035	0.002	39.116	15.621	17.955
DPX-2			39.353	0.005	15.6	0.002	17.921	0.002	39.011	15.595	17.819
DPX-3			39.299	0.006	15.611	0.003	17.94	0.003	39.039	15.607	17.865
DPX-4			39.282	0.009	15.604	0.004	17.926	0.004	38.963	15.599	17.82
DPX-5			39.393	0.006	15.614	0.002	17.962	0.002	39.023	15.608	17.848

Note: The formation age of trachyte porphyry is from unpublished U–Pb data.

6. Discussion

6.1. Properties of Ore-Forming Fluids

The primary L-dominated fluid inclusions occurring in ores of stages II and III were measured in this study. In the main ore stage, the homogenization temperatures of L-dominated fluid inclusions range from 113 to 162 °C, which indicate that the main ore-forming fluids belong to the low-temperature fluid system [29]. The homogenization

temperatures of L-dominated fluid inclusions in the late quartz–calcite stage decrease (106–143 °C), indicating the occurrence of fluid cooling, which is an important control on ore deposition [30]. The salinities of fluids also decrease from the main ore stage (average 7.2 wt% NaCl equiv.) to the late stage (average 6.1 wt% NaCl equiv.), which is similar to those of the low-sulfidation epithermal gold deposits worldwide (commonly <5 wt% NaCl equiv.; [22]). Previous studies have indicated that the ore-forming fluids of the Dongpuzi gold deposit are NaCl–H₂O-dominated type [3]. Therefore, the ore-forming fluids of the Dongpuzi gold deposit are a low-temperature (113 to 162 °C) and low-salinity (average 7.2 wt% NaCl equiv.) NaCl–H₂O fluid system and fluid cooling may be an important factor in the formation of this gold deposit.

6.2. Origin of Ore-Forming Fluids

The δD_{water} and calculated $\delta^{18}O_{\text{water}}$ values of the fluid trapped in quartz from the Dongpuzi ore stage II are -103.3‰ to -96.1‰ and -14.71‰ to -13.31‰ , respectively, which are consistent with corresponding values of the hydrothermal fluids from ore stage III (Table 3). These data are plotted in or close to the meteoric water line in a δD – $\delta^{18}O_{\text{H}_2\text{O}}$ diagram, indicating that the ore-forming fluids of the Dongpuzi deposit were predominantly derived from meteoric water, with little indication of magmatic water (Figure 7a). Furthermore, these data are compatible with those of fluids from low-sulfidation epithermal systems worldwide (Figure 7a) [22].

Three calcite samples from stage III have measured $\delta^{13}C_{\text{V-PDB}}$ values, ranging from -4.5‰ to -4.2‰ , close to those of igneous- or mantle-derived CO₂ (-2‰ to -7‰ ; [24]) and of mixed crustal sources (average -5‰ ; [27]), indicating that the carbon in the Dongpuzi gold deposit was derived from either the mantle or a mixed crustal source. This is also shown in the $\delta^{13}C$ – $\delta^{18}O$ diagram (Figure 7b). The variations in C–O isotope compositions are likely affected by the fluid–rock interaction during the evolution of the ore-forming fluids [31].

6.3. Sources of Sulfur and Lead

Under temperatures lower than 350 °C and reduced hydrothermal conditions where H₂S is the dominant sulfur species in the fluid, the $\delta^{34}S$ values of sulfide minerals will represent the overall S isotope composition of the hydrothermal fluid (i.e., $\delta^{34}S_{\Sigma S} \approx \delta^{34}S_{\text{sulfide}}$) [27]. The Dongpuzi gold mineralization is formed under low temperatures, as stated above. The mineralogical observations indicate that the ores are mainly composed of pyrite, chalcopyrite, and sphalerite, which are generally formed in a reducing environment, and no sulfate minerals were found. Therefore, the average $\delta^{34}S$ values of sulfide minerals approximate the sulfur isotopic compositions of hydrothermal fluid. Five pyrite samples from gold ores yield $\delta^{34}S$ values of $+4.1\text{‰}$ to $+6.6\text{‰}$ (Figure 8a and Table 4), basically consistent with the $\delta^{34}S_{\text{V-CDT}}$ values of $+2.39\text{‰}$ to $+7.99\text{‰}$ reported by Zhang et al. [15]. These values are a little higher than those of magmatic reservoirs ($0\text{‰} \pm 3\text{‰}$; [27]) but lower than those of the schist and granulite of the Gaixian Formation ($+10.0\text{‰}$ to $+17.0\text{‰}$; [26]; Figure 8b). Therefore, the sulfur in ores was predominantly derived from the magmatic system, with some combination of metamorphic rocks of the Gaixian Formation for the Dongpuzi deposit.

The pyrite samples from the Dongpuzi ores yield homogeneous $^{206}\text{Pb}/^{204}\text{Pb}$ ratios of 17.918–18.07, $^{207}\text{Pb}/^{204}\text{Pb}$ ratios of 15.595–15.641, and $^{208}\text{Pb}/^{204}\text{Pb}$ ratios of 38.557–38.827 (Table 4). The Pb isotope data are all plotted adjacent to the orogen line on a $^{207}\text{Pb}/^{204}\text{Pb}$ – $^{206}\text{Pb}/^{204}\text{Pb}$ diagram (Figure 8b), suggesting a mixed crust–mantle source. Furthermore, the Pb isotope compositions of pyrite are consistent with those of the ore-hosting trachyte porphyry and intermediate–basic volcanic rocks of the Xiaoling Formation (Figure 8b). Previous studies have demonstrated that the Early Cretaceous intermediate–basic volcanic rocks of the Xiaoling Formation in the Xiuyan area were formed by partial melting of ancient lithospheric mantle, metasomatized by subduction fluids [28]. Therefore, the volcanic rocks of the Xiaoling Formation, especially the ore-hosting trachyte porphyry, are closely related to the Dongpuzi gold mineralization.

6.4. Ore genesis and the Metallogenic Model

As stated above, the Dongpuzi gold deposit is located in the southern margin of the Shaozihe volcanic fault basin. The gold orebodies at the Dongpuzi deposit are hosted within the trachyte porphyry and are structurally controlled by the NE–SW- to NNE–SSW-trending faults and fracture alteration zones. The ores are characterized by quartz veins, quartz veinlets, quartz stockworks, or miarolitic structures, indicating that the gold mineralization occurred on the surface or near the surface [32]. The ore mineral assemblage from the mineralogical observations is dominated by pyrite, chalcopyrite, and sphalerite, indicating a low-sulfidation state [33]. The wall-rock alterations include sericitization, silicification, carbonatization, kaolinization, and chloritization and display clear spatial zonation similar to low-sulfidation epithermal deposits [15]. Fluid inclusion studies indicate that the mineralizing fluid is characterized by a low temperature (average 134 °C, <150 °C) and salinity (average 7.2 wt% NaCl equiv.) with a meteoric source (Figure 7a). These characteristics are similar to those of typical low-sulfidation epithermal gold deposits in China and worldwide [34–36]. Therefore, the Dongpuzi gold deposit belongs to a typical low-sulfidation epithermal gold deposit in the Liaodong area.

During the Early Cretaceous period, the Paleo-Pacific Ocean Plate subducted beneath the Eurasian plate [37,38] and subsequently underwent a transformation from compression–subduction to slab rollback–extension in the east of the NCC [38,39], which triggered intense magmatism and related mineralization, as well as a series of extensional structures, such as metamorphic core complex (Liaonan–Wanfu), half graben basins (Benxi, Tongyuanpu, and Dandong), and detachment fault systems (Huanghuadianzi–Dayingzi–Shaozihe) in the Liaodong Peninsula [11,13,40–43]. The retreating of the subducted Paleo-Pacific Ocean Plate induced the underplating of the asthenospheric mantle [38], which further triggered partial melting of the ancient lithospheric mantle in the east of the NCC [28,40,44,45]. The produced mantle-derived magmas were metasomatized by subducting oceanic slab-derived fluids [28]. Through fractional crystallization, the intermediate–basic volcanic rocks of the Xiaoling Formation in the Shaozi River fault basin were thus generated in the Xiuyan area [28], accompanied by intrusion of the ore-hosting trachyte porphyry. The new hydrogen, oxygen, and carbon isotope data indicate that the ore-forming fluids were derived from meteoric water, with important input of mantle-derived carbon. The sulfur and lead isotopes suggest that the sulfur and lead were mainly leached from the ore-hosting trachyte porphyry, with some contributions of the basement rocks (metamorphic rocks of the Gaixian Formation). The trachyte porphyry supplied high heat flow, drove shallow meteoric water, and remobilized metallogenic materials (sulfur, lead, and carbon) from the volcanic rocks (mainly trachyte porphyry) and metamorphic rocks of the Gaixian Formation (Figure 9). The episodic temperature and salinity drops in the mineralizing fluid perhaps resulted in the formation of the Dongpuzi gold deposit.

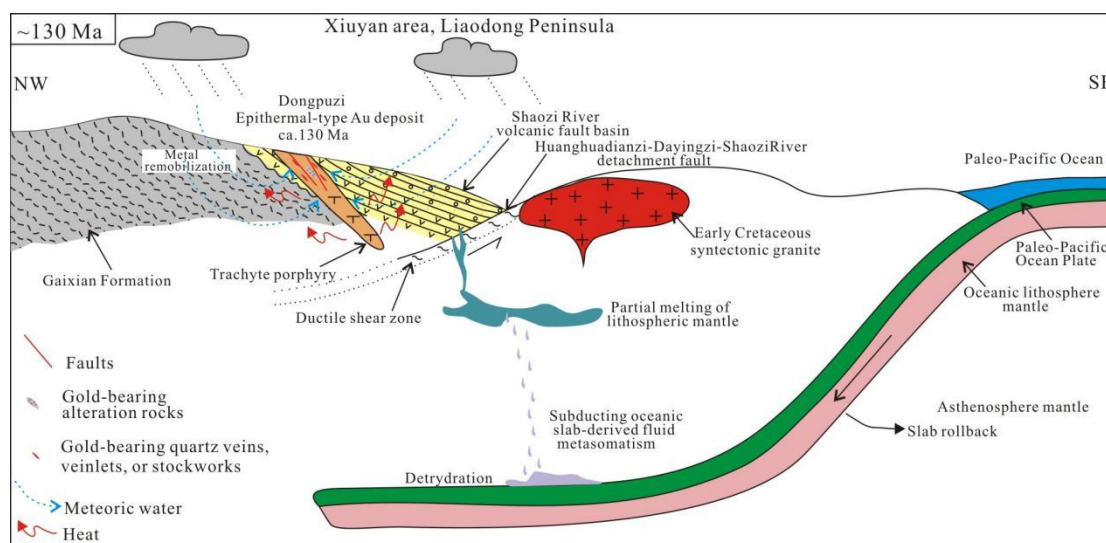


Figure 9. Schematic model explaining the formation of the Dongpuzi gold deposit (the geodynamic setting of the Early Cretaceous in the eastern NCC is after [11,13,40–43]; the diagenesis of intermediate-basic rocks of the Xiaoling Formation is after [28]; the age of ~130 Ma is taken from unpublished U–Pb data of the trachyte porphyry).

7. Conclusions

- (1) The Dongpuzi gold deposit was hosted within the Early Cretaceous trachyte porphyry and controlled by the NE–SW- to NNE–SSW-trending faults and fracture zones, with three mineralization stages, i.e., quartz–pyrite, quartz–sulfide, and quartz–calcite stages.
- (2) Fluid inclusion studies indicate that the Dongpuzi gold mineralization was precipitated from an epithermal fluid system with low temperatures (113 to 162 °C) and low salinity (average 7.2 wt% NaCl equiv.) and fluid cooling may be an important factor in the formation of this gold deposit.
- (3) The hydrogen, oxygen, and carbon isotopes indicate that the ore-forming fluids were sourced from meteoric water and the carbon in fluids is mainly derived from the magma. The sulfur and lead isotopic compositions suggest that the ore-forming materials were mainly derived from the host trachyte porphyry and volcanic rocks of the Xiaoling Formation, with some contributions of Paleoproterozoic metamorphic rocks of the Gaixian Formation.
- (4) The Dongpuzi deposit is a typical low-sulfidation epithermal gold deposit in the Liaodong area, which was formed under an extensional setting related to the Early Cretaceous lithospheric extension and thinning of the east of NCC, induced by subduction and retreat of the Paleo-Pacific Ocean Plate.

Author Contributions: Conceptualization, C.C. and T.W.; methodology, J.Z.; formal analysis, Q.S.; investigation, D.S., D.L., Z.Y. and J.Z.; writing—original draft preparation, C.C. and Q.S.; writing—review and editing, C.C., T.W. and D.S.; visualization, Q.S.; supervision, C.C. and T.W.; funding acquisition, D.S. and Z.Y. All authors have read and agreed to the published version of the manuscript.

Funding: This research was funded by the Geological Survey Project of China, grant numbers DD20221695, DD20221678, and DD20190379, and the National Key Research and Development Program of China, grant numbers 2018YFC0603804 and 2016YFC0600108.

Acknowledgments: We are grateful to the anonymous reviewers for their constructive comments, which greatly helped in improving our paper. We would like to thank Xin-hui Ma and Mu Liu from the Analytical Laboratory of the Beijing Research Institute of Uranium Geology, Beijing, China, for their help during the fluid inclusion and C–H–O–S–Pb isotope analyses.

Conflicts of Interest: The authors declare no conflict of interest.

References

1. Liu, J.; Zhang, L.J.; Wang, S.L.; Li, T.G.; Yang, Y.; Liu, F.X.; Li, S.H.; Duan, C. Formation of the Wulong gold deposit, Liaodong gold Province, NE China: Constraints from zircon U–Pb age, sericite Ar–Ar age and H–O–S–He isotopes. *Ore Geol. Rev.* **2019**, *109*, 130–143. [[CrossRef](#)]
2. Chen, C.; Li, D.T.; Wu, T.T.; Zhao, Y.; Zhao, C.Q.; Yang, J.L.; Gu, Y.C. Genesis of gold deposits in the Wulong orefield, Liaodong Peninsula, North China Craton: Constraints from ore deposit geology, REE, and C–H–O–S–Pb isotopes. *Geol. J.* **2020**, *55*, 5914–5933. [[CrossRef](#)]
3. Zhang, P.; Kou, L.L.; Zhao, Y.; Bi, Z.W.; Sha, D.M.; Han, R.P.; Li, Z.M. Genesis of the Wulong gold deposit, Liaoning Province, NE China: Constraints from noble gases, radiogenic and stable isotope studies. *Geosci. Front.* **2020**, *11*, 547–563. [[CrossRef](#)]
4. Yu, G.; Zeng, Q.D.; Frimmel, H.E.; Wang, Y.B.; Guo, W.K.; Sun, G.T.; Zhou, T.C.; Li, J.P. Genesis of the Wulong gold deposit, northeastern North China Craton: Constraints from fluid inclusions, H–O–S–Pb isotopes, and pyrite trace element concentrations. *Ore Geol. Rev.* **2018**, *102*, 313–337. [[CrossRef](#)]
5. Chen, J. Geological characteristics and ore-forming control of the Dongpuzi gold deposit in Liaoning Province. *Gold J.* **2000**, *2*, 1–5. (In Chinese)
6. Zhang, B.C.; Qin, G.J.; Wang, F.G. Fluid inclusions of Dongpuzi gold deposit in Xiuyan county, Liaoning Province. *Geoscience* **2002**, *16*, 26–31. (In Chinese)
7. Jiang, Y.Z. Geochemical characteristics of the Dongpuzi gold deposit in Liaoning Province. *Non-Ferr. Min. Metall.* **2017**, *33*, 4–8. (In Chinese)
8. Zhao, G.C.; Sun, M.; Wilde, S.A.; Li, S.Z. Late Archean to Paleoproterozoic evolution of the North China Craton: Key issues revisited. *Precambrian Res.* **2005**, *136*, 177–202. [[CrossRef](#)]
9. Liu, J.Y.; Chen, H.; Sha, D.; Wang, H. The inner zone of the Liaoji Paleorift: Its early structural styles and structural evolution. *J. Asian Earth Sci.* **1997**, *15*, 19–31. [[CrossRef](#)]
10. Li, S.Z.; Zhao, G.C. SHRIMP U–Pb zircon geochronology of the Liaoji granitoids: Constraints on the evolution of the Paleoproterozoic Jiao-Liao-Ji belt in the Eastern Block of the North China Craton. *Precambrian Res.* **2007**, *158*, 1–16. [[CrossRef](#)]
11. Shen, L.; Liu, J.L.; Hu, L.; Ji, M.; Guan, H.M. The Dayingzi detachment fault system in Liaodong Peninsula and its regional tectonic significance. *Sci. China Earth Sci.* **2011**, *41*, 437–451. (In Chinese) [[CrossRef](#)]
12. Wu, F.Y.; Lin, J.Q.; Wilde, S.A.; Zhang, X.O.; Yang, J.H. Nature and significance of the Early Cretaceous giant igneous event in eastern China. *Earth Planet. Sci. Lett.* **2005**, *233*, 103–119. [[CrossRef](#)]
13. Liu, J.L.; Ji, M.; Shen, L.; Guan, H.M. Early Cretaceous extensional structures in the Liaodong Peninsula: Structural associations, geochronological constraints and regional tectonic implications. *Sci China Earth Sci* **2011**, *54*, 823–842. (In Chinese) [[CrossRef](#)]
14. Liaoning Nonferrous Shenyang Geological Exploration Institute. Geological Survey Report of the Dongpuzi gold deposit in Xiuyan County, Liaoning Province. 1998; (Unpublished).
15. Zhang, B.C.; Li, L.; Tan, G.J. Study on geological feature and genesis of the Dongpuzi gold deposit, Liaoning, China. *Gold Geol.* **2002**, *8*, 29–36. (In Chinese)
16. O'Neil, J.R.; Russel, R.D. Discrimination in solid source lead isotope abundance measurement. *Earth Planet. Sci. Lett.* **1970**, *8*, 331–336. [[CrossRef](#)]
17. Guo, L.N.; Goldfarb, R.J.; Wang, Z.L.; Li, R.H.; Chen, B.H.; Li, J.L. A comparison of Jiaojia- and Linglong-type gold deposit ore-forming fluids: Do they differ? *Ore Geol. Rev.* **2017**, *88*, 511–533. [[CrossRef](#)]
18. Potter, R.W.; Clyne, M.A. Freezing point depression of aqueous sodium chloride solution. *Econ. Geol.* **1978**, *73*, 284–285. [[CrossRef](#)]
19. Clayton, R.N.; O'Neil, J.R.; Mayeda, T.K. Oxygen isotope exchange between quartz and water. *Geophys. Res.* **1972**, *77*, 3057–3067. [[CrossRef](#)]
20. Taylor, H.P. The application of oxygen and hydrogen isotope studies to problems of hydrothermal alteration and ore deposit. *Econ. Geol.* **1974**, *69*, 843–883. [[CrossRef](#)]
21. Hedenquist, J.W.; Lowenstern, J.B. The role of magmas in the formation of hydrothermal ore deposits. *Nature* **1994**, *370*, 519–527. [[CrossRef](#)]
22. Simmons, S.F.; White, N.C.; John, D.A. Geological Characteristics of Epithermal Precious and Base Metal Deposits. In *Economic Geology: One Hundredth Anniversary Volume*; Hedenquist, J.W., Thompson, J.F.H., Goldfarb, R.J., Richards, J.P., Eds.; Society of Economic Geologists: Littleton, CO, USA, 2005; pp. 485–522.
23. Li, L.; Li, S.R.; Santosh, M.; Zhu, J.; Suo, X.J. Early Jurassic decratonic gold metallogenesis in the eastern North China Craton: Constraints from S–Pb–C–D–O isotopic systematics and pyrite Rb–Sr geochronology of the Guilaizhuang Te–Au deposit. *Ore Geol. Rev.* **2018**, *92*, 558–568. [[CrossRef](#)]
24. Hoefs, J. *Stable Isotope Geochemistry*, 6th ed.; Springer: Berlin/Heidelberg, Germany, 2009; pp. 130–135.
25. Ray, J.S.; Ramesh, R.; Pande, K. Carbon isotopes in Kerguelen plume derived carbonatites: Evidence for recycled inorganic carbon. *Earth Planet. Sci. Lett.* **1999**, *170*, 205–214. [[CrossRef](#)]
26. Zhao, H.Z.; Yang, S.S.; Li, H. Geologic features of Baiyun gold deposit and discussion of the genesis. *Non-Ferrous Min. Metall.* **2009**, *25*, 4–8. (In Chinese)
27. Ohmoto, H.; Rye, R.O. Isotopes of sulfur and carbon. In *Geochemistry of Hydrothermal Ore Deposits*, 2nd ed.; Barnes, H.L., Ed.; John Wiley & Sons Inc.: New York, NY, USA, 1979; pp. 509–567.

28. Zhou, H.; Pei, F.P.; Xu, W.L.; Wei, J.Y.; Wang, Y.P. Petrogenesis of the Early Cretaceous volcanic rocks from the northeastern part of the North China Craton: Elemental and Sr-Nd-Pb isotopic constraints. *Lithos* **2021**, *392*, 393106149.
29. Lindgren, W. *Mineral Deposits*; McGraw-Hill Book Company, Inc.: New York, NY, USA; London, UK, 1933.
30. Fournier, R.O. Hydrothermal process related to movement of fluid from plastic into brittle rock in the magmatic–epithermal environment. *Econ. Geol.* **1999**, *94*, 1193–1211. [[CrossRef](#)]
31. Gu, F.H.; Zhang, Y.M.; Peng, Y.W.; Wang, J.L.; Liu, R.P. Geology, fluid inclusions and S-Pb-C-O isotopes of the Kuokuqueke Fe-Cu skarn deposit in Western Tianshan, China. *Ore Geol. Rev.* **2022**, *145*, 104896. [[CrossRef](#)]
32. Chen, Y.J.; Ni, P.; Fan, H.R.; Pirajno, F.; Lai, Y.; Su, W.C.; Zhang, H. Diagnostic fluid inclusions of different types hydrothermal gold deposits. *Acta Petrol. Sin.* **2007**, *23*, 2085–2108. (In Chinese)
33. Hedenquist, J.W.; Arribas, A., Jr.; Gonzalez-Urien, E. Exploration for epithermal gold deposits. *Rev. Econ. Geol.* **2000**, *13*, 245–277.
34. Ma, Y.; Jiang, S.Y.; Frimmel, H.E. Metallogeny of the Late Jurassic Qicun epithermal gold deposit in southern China: Constraints from geochronology, fluid inclusions, and H-O-S-Pb isotopes. *Ore Geol. Rev.* **2022**, *142*, 104688. [[CrossRef](#)]
35. Najaran, M.; Mehrabi, B.; Siani, M.G. Mineralogy, hydrothermal alteration, fluid inclusion, and O-H stable isotopes of the SiahJangal-Sar Kahno epithermal gold deposit, SE Iran. *Ore Geol. Rev.* **2020**, *125*, 103689. [[CrossRef](#)]
36. Li, S.N.; Ni, P.; Bao, T.; Wang, G.G.; Chi, Z.; Li, W.S.; Zhu, R.Z.; Dai, B.Z.; Xiang, H.L. Geological, fluid inclusion, and H-O-S-Pb isotopic studies of the Xiaban epithermal gold deposit, Fujian Province, southeast China: Implications for ore genesis and mineral exploration. *Ore Geol. Rev.* **2020**, *117*, 103280. [[CrossRef](#)]
37. Zhu, R.X.; Fan, H.R.; Li, J.W.; Meng, Q.R.; Li, S.R.; Zeng, Q.D. Decratonic gold deposits. *Sci. China Earth Sci.* **2015**, *58*, 1523–1537. [[CrossRef](#)]
38. Zheng, J.P.; Dai, H.K. Subduction and retreating of the western Pacific plate resulted in lithospheric mantle replacement and coupled basin-mountain respond in the North China Craton. *Sci. China Earth Sci.* **2018**, *61*, 406–424. [[CrossRef](#)]
39. Zheng, Y.F.; Xu, Z.; Zhao, Z.F.; Dai, L.Q. Mesozoic mafic magmatism in North China: Implications for thinning and destruction of cratonic lithosphere. *Sci. China Earth Sci.* **2018**, *61*, 353–385. [[CrossRef](#)]
40. Wu, F.Y.; Yang, J.H.; Xu, Y.G.; Wilde, S.A.; Walker, R.J. Destruction of the North China Craton in the Mesozoic. *Annu. Rev. Earth Planet. Sci.* **2019**, *47*, 173–195. [[CrossRef](#)]
41. Yang, J.H.; Wu, F.Y.; Chung, S.L.; Wilde, S.A.; Davis, G.A. Rapid exhumation and cooling of the Liaonan metamorphic core complex: Inferences from $^{40}\text{Ar}/^{39}\text{Ar}$ thermochronology and implications for Late Mesozoic extension in the eastern North China Craton. *Geol. Soc. Am. Bull.* **2007**, *119*, 1405–1414. [[CrossRef](#)]
42. Liu, J.L.; Guan, H.M.; Ji, M.; Hu, L. Late Mesozoic metamorphic core complexes: New constraints on lithosphere thinning in North China. *Prog. Nat. Sci.* **2006**, *16*, 633–638.
43. Qian, Y.; Sun, J.L.; Li, Y.J.; Yu, N.; Liu, J.L.; Li, B.L.; Sun, F.Y. Geochronology, geochemistry and metallogenic dynamics of gold-polymetallic deposits in Xicha region, the northeastern margin of the North-China Platform. *Acta Petrol. Sin.* **2020**, *36*, 1127–1150. (In Chinese)
44. Pei, F.P.; Xu, W.L.; Yang, D.B.; Yu, Y.; Wang, W.; Zhao, Q.G. Geochronology and geochemistry of Mesozoic mafic-ultramafic complexes in the southern Liaoning and southern Jilin Provinces, NE China: Constraints on the spatial extent of destruction of the North China Craton. *J. Asian Earth Sci.* **2011**, *40*, 636–650. [[CrossRef](#)]
45. Ma, Q.; Xu, Y.G.; Zheng, J.P.; Griffin, W.L.; Hong, L.B.; Ma, L. Coexisting Early Cretaceous High-Mg andesites and adakitic rocks in the North China Craton: The role of water in intraplate magmatism and cratonic destruction. *J. Petrol.* **2016**, *7*, 1279–1308. [[CrossRef](#)]